Supplementary Information

Se self-doped $Ni(OH)_2$ for efficient urea oxidation reaction

Shenyi Song[a], Xingyu Huang[a], Yun Yang[b*], Ligang Feng[a*]

a. School of Chemistry and Chemical Engineering, Yangzhou University, Yangzhou 225002, P.R. China. Email: ligang.feng@yzu.edu.cn; fenglg11@gmail.com (L Feng)

b. Nanomaterials and Chemistry Key Laboratory, Wenzhou University, Wenzhou, China. E-mail: bachier@163.com

1. Materials and chemicals

Nickel(II) acetate tetrahydrate ($Ni(Ac)_2 \cdot 4H_2O$), sodium selenite ($NaSeO_3$), ethylene glycol ($C_2H_6O_2$), Urea($CO(NH_2)_2$), and potassium hydroxide (KOH) were procured from Shanghai Aladdin Biochemical Technology Co., Ltd. A 5 wt.% Nafion ionomer was obtained from Sigma-Aldrich. Absolute ethanol (C_2H_6O) was acquired from Beijing Chemical Works. All chemicals used in this study were of analytical grade and were utilized without further purification. Ultrapure water with a resistance of 18.2 MΩ (Thermo Fisher Scientific Co., LTD, USA) was used throughout all experiments.

2. Materials fabrication

2.1. Synthesis of Se-Ni(OH)$_2$

The preparation method for a Ni-Se molar ratio of 2:1 involves adding $Ni(Ac)_2 \cdot 4H_2O$ (2 mmol), Na_2SeO_3 (1 M, 1 mL), and $C_2H_6O_2$ (50 mL) to a three-neck flask, followed by microwave heating (600 W, 100°C, 5 minutes), filtering three times, and vacuum drying. By varying the molar amount of Na_2SeO_3, different Ni-Se molar ratios can be achieved.

2.2. Synthesis of Ni(OH)$_2$

$Ni(Ac)_2 \cdot 4H_2O$ (2 mmol), KOH (4 mmol) into 50 ml of ultrapure water, stand for 12 h, filter three times, and vacuum dry.

3. Physical characterization

3.1. Fundamental Physical Characterizations

The crystalline structure was elucidated via X-ray diffraction (XRD, Bruker D8 Advance), employing a copper Kα radiation source (λ = 1.5405 Å) under operating conditions of 40 kV and 40 mA, with a scan rate of 5° min^{-1}. The chemical state of the catalyst surface was probed using X-ray photoelectron spectroscopy (XPS) with the Kα radiation source. The morphological features of the catalyst were examined through scanning electron microscopy (SEM, FEI Sirion-200). The microstructural attributes and particle size distribution of the Se-$Ni(OH)_2$ material were meticulously analyzed utilizing transmission electron microscopy (TEM, FEI TECNAI, 200 kV), high-resolution transmission electron microscopy (HRTEM), scanning transmission electron microscopy (STEM) in high-angle annular dark-field (HAADF) mode, and energy-dispersive X-ray spectroscopy (EDS).

3.2. In situ synchrotron radiation Fourier transform infrared measurements.

Electrochemical attenuated total reflectance infrared (FT-IR) measurements were conducted on an Au/Si hemispherical prism cast with a Se-$Ni(OH)_2$ catalyst layer, using a Nicolet iS50 spectrometer (Thermo Fisher Scientific, USA) equipped with an MCT detector. The p-polarized infrared radiation was incident at an angle of approximately 70° with a spectral resolution of 4 cm^{-1}. The catalyst ink was transferred onto the electrochemically pre-cleaned Au film using a pipette. All spectra were presented in absorbance units as $-\log(I/I_0)$, where I and I_0 represent the reflected radiation intensities of the sample and reference spectra, respectively.

4. Preparation of working electrode

All the electrochemical measurements were carried out with a Bio-Logic VSP electrochemical workstation (Bio-Logic, France) and a conventional three-electrode system. The working electrode consisted of a catalyst-coated glassy carbon electrode with an inner diameter of 3 mm and an outer diameter of 4 mm. A graphite rod and a Hg/HgO electrode were employed as counter and reference electrodes, respectively. The accuracy of the reference electrode was carefully checked before and after the tests to ensure precise measurements. All the potentials were converted and referred to a reversible hydrogen electrode (RHE) unless otherwise noted. The current was reported by normalizing the current to the geometric surface area of the electrode unless otherwise noted. The preparation of the catalyst ink involved dispersing 5 mg of the catalyst into a 1 mL solution containing 950 μL ethanol and 50 μL Nafion, followed by sonication for 30 minutes to achieve a homogeneous ink. Subsequently, 10 μL of the catalyst ink was pipetted and deposited onto a pre-cleaned glassy carbon electrode with a geometric surface area of 0.07 cm^2, and allowed to dry at room temperature. All electrolytes for urea oxidation contained 1 mol L^{-1}potassium hydroxide and 0.33 mol L^{-1} urea solution.

5. Electrochemical measurements

5.1. OER performance testing

Circular voltammetry (CV) at 1mol L^{-1} potassium hydroxide solution with a voltage range of 1.04 V - 1.7 V and a scan rate of 10 mV s^{-1}. The electrochemical surface area (ECSA) was calculated by using the charge required to reduce NiOOH to $Ni(OH)_2$ in the backward scan of CV curves in KOH solution according to the formula $ECSA=Q/0.257*m^1$, in which the charge (Q) represented the cathodic reduction peak of Ni^{3+}/Ni^{2+}. The Q=peak area (S)/scan rate (v), where S was estimated via integrating the area of the reduction peak of the CV diagram. The 0.257 mC cm^{-2} is the charge

required to form a monolayer of Ni^{2+}, and m is the loading amount of the catalyst. The intrinsic activity of all the catalysts was revealed by normalizing the current to the ECSA to evaluate the catalytic efficiency of the active sites.

5.2. Urea oxidation tests

The catalytic performance of the urea oxidation catalyst was detected by cyclic voltammetry (CV) in 1 mol L^{-1} potassium hydroxide and 0.33 mol L^{-1} urea solutions with a voltage range of 1.04 V~1.54 V and a scanning rate of 1-10 mV s^{-1}. By plotting the peak current density versus the square root of scan rate, a linear relationship can be obtained following the equation of $i_p=2.99\times10^5n(an')^{1/2}C_\infty D_0^{1/2}v^{1/2}$, where i_p is the peak current density, n is the electron number for the total reaction, a is the electron transfer coefficient of the rate-determining step, n' is the electron number transferred in the rate-determining step, C_∞ is the bulk concentration of the reactant, D_0 is the diffusion coefficient, v is the potential scan rate. In same reaction system, the parameters of n, C_∞ and D_0 are equal, so the slope is only determined by an'. Thus, the higher the slope, the faster the reaction kinetics.

Urea oxidation time amp (CA) was tested at 1.35 V *vs*.RHE for 100 h. The Tafel slope is calculated from formula (2):$\eta = a + b \log (j)$[4]

Where η is the overpotential (mV), b is the Tafel slope, and j is the current density. The b value reflects the electrochemical dynamic relationship, and the smaller the b value, the faster the chemical reaction kinetics.

The electrochemical impedance spectroscopy (EIS) was recorded in the above three-electrode cell at the frequency ranging from 1000 kHz to 10 mHz with 12 points per decade. Regulating different amplitude potential signals 0.24 V-0.5 V, The Nyquist and Bode plots were obtained at different voltages.

6. Theoretical calculations

Spin-polarized density functional theory (DFT) calculations were performed using the Vienna Ab initio Simulation Package (VASP) [5] to investigate the urea oxidation reaction (UOR) processes on the synthesized materials. The Perdew-Burke-Ernzerhof (PBE) functional was employed within the DFT framework, utilizing the projector augmented wave (PAW) method with a cutoff energy of 380 eV. Electronic self-consistency was assumed when the energy change was less than 10^{-5} eV, and geometric optimization was considered converged when the energy change

was below 0.05 eV/Å. The adsorption energy ($E_{ads)}$ was calculated using the following formula[6]:

$E_{ads} = E_{A/surf} - E_{surf} - E_{A(g)}$

The adsorption energy (E_{ads}) has been calculated using the formula The E_{total}, $E_{substrate,}$ and $E_{adsorbate}$ represent the energy of adsorption structure, substrate, and adsorbate, respectively.[7]

During the structural optimization, k-point sampling was conducted using a 3×3×2 grid in the Brillouin zone. The bottom two atomic layers were fixed, while the top two atomic layers were allowed to relax, constructing the $Ni(OH)_2$ (110) surface. A vacuum gap of 10 Å was established in the models of both pure $Ni(OH)_2$ and Se-doped $Ni(OH)_2$. With a cutoff energy of 380 eV, the density of states (DOS) post-Se doping was calculated, as well as the adsorption energies of urea and carbon dioxide molecules on the catalyst surface.

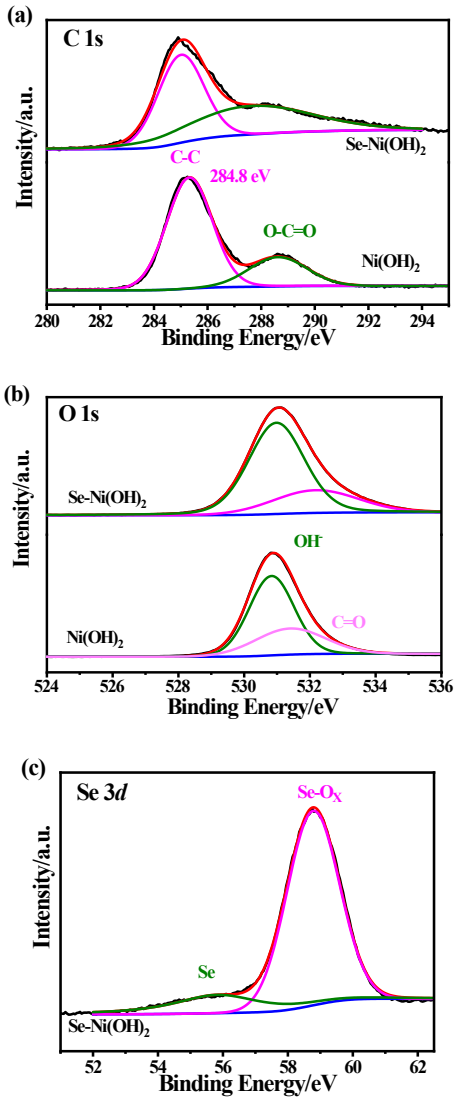

Fig.S1. XPS spectra of C 1s (a), O1s (b),Se 3d (c)of catalysts.

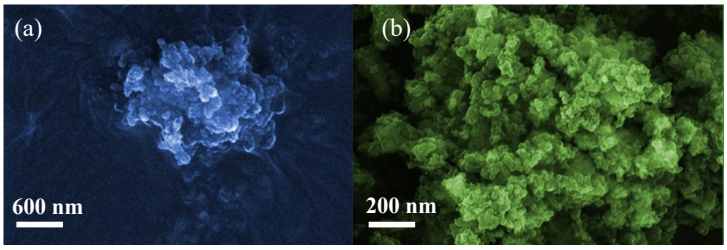

Fig.S2. SEM images of Se-Ni$(OH)_2$

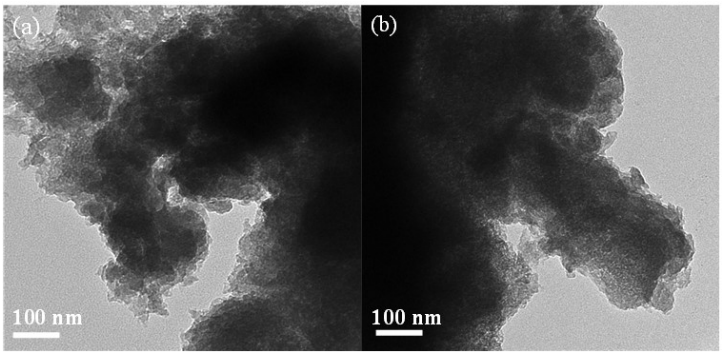

Fig.S3. TEM images of Se-Ni$(OH)_2$

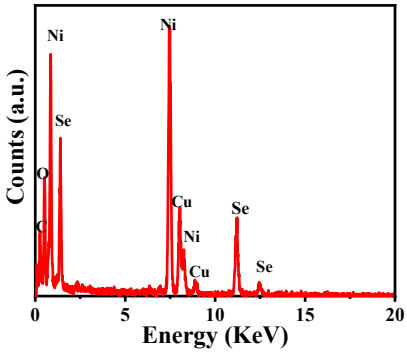

Fig.S4. EDS spectrum of the Se-Ni(OH)$_2$

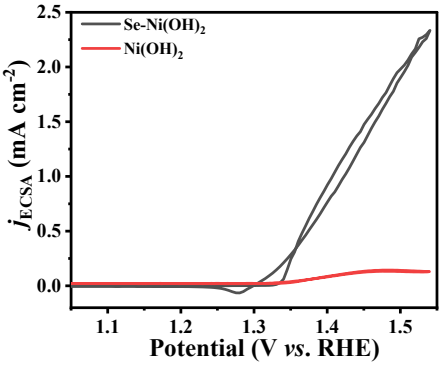

Fig. S5. Specific activity polarization curves of Ni(OH)$_2$ and Se-Ni(OH)$_2$.

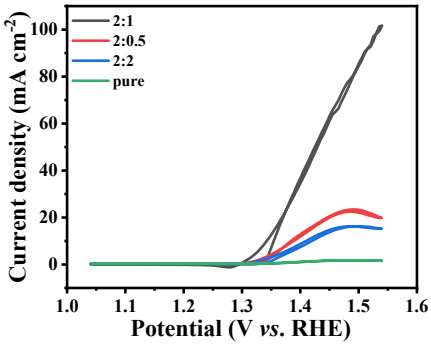

Fig. S6. Cyclic voltammetry curves in 1 M KOH with 0.33 M urea at 5 mV s^{-1} for Ni-Se with different feed ratios, and the 2:1 means the Se-doped $Ni(OH)_2$ in the text (Pure represents $Ni(OH)_2$ without Se doping).

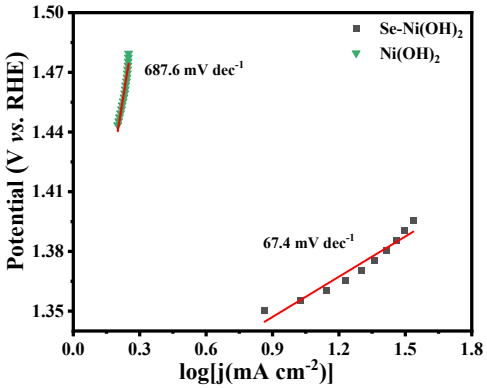

Fig. S7. Tafel plots for the $Ni(OH)_2$ and Se-$Ni(OH)_2$ samples.

Note： the Tafel value of 687 mV/dec does not have a clear meaning for the catalysis process due to the very bad performance.

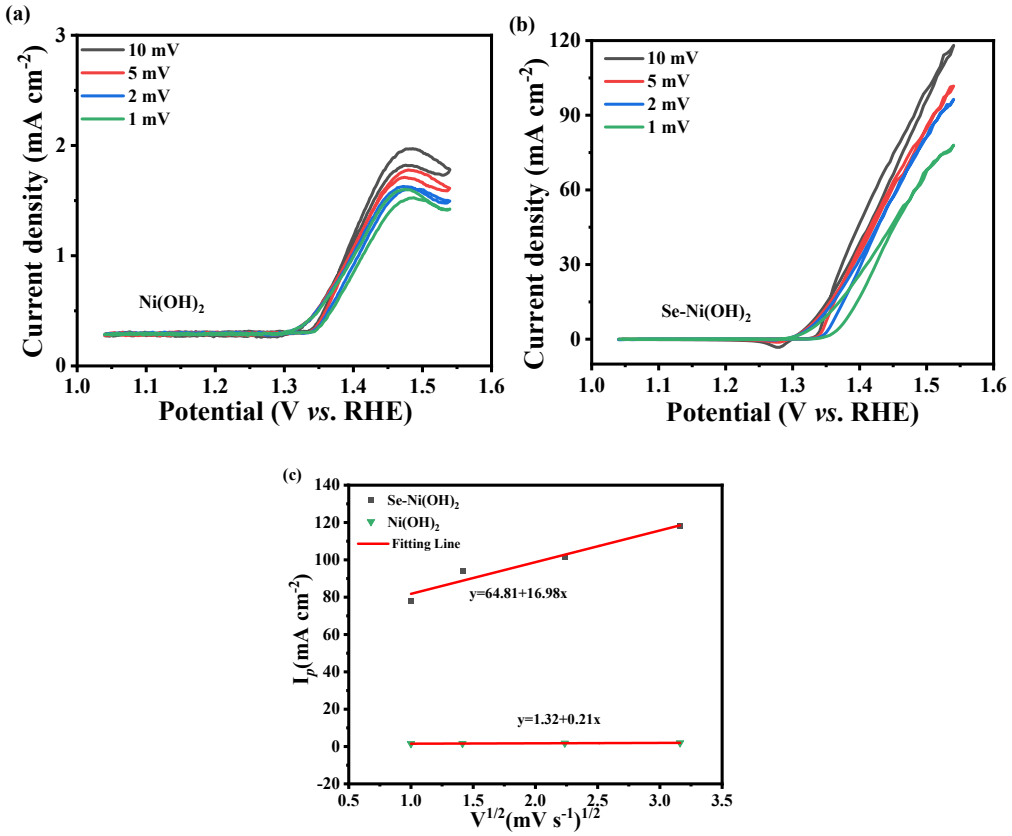

Fig. S8 Cyclic voltammetry curves in 1 M KOH solution with 0.33 M urea at different scan rates of 1, 2, 5, and 10 mV s^{-1} for (a) $Ni(OH)_2$ and (b)Se-$Ni(OH)_2$ (c) the plot of peak current density vs. the square root of scan rate for all the samples.

8

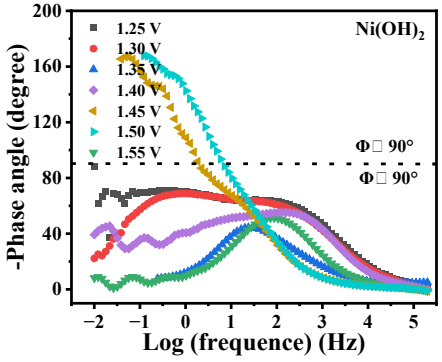

Fig. S9. $Ni(OH)_2$ Bode diagram in 1 M KOH solution with 0.33 M urea at different voltages.

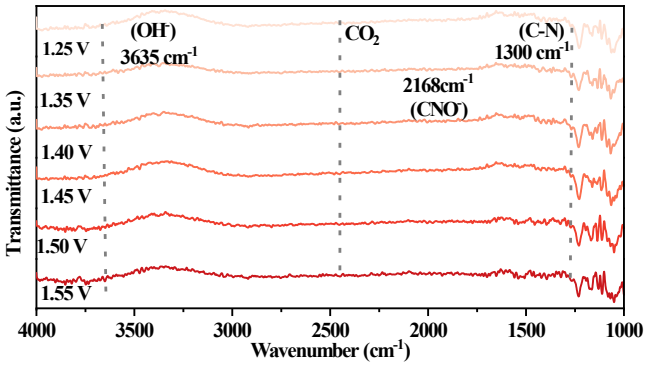

Fig. S10. In situ FT-IR spectra of the $Ni(OH)_2$ catalysts at different applied potentials.

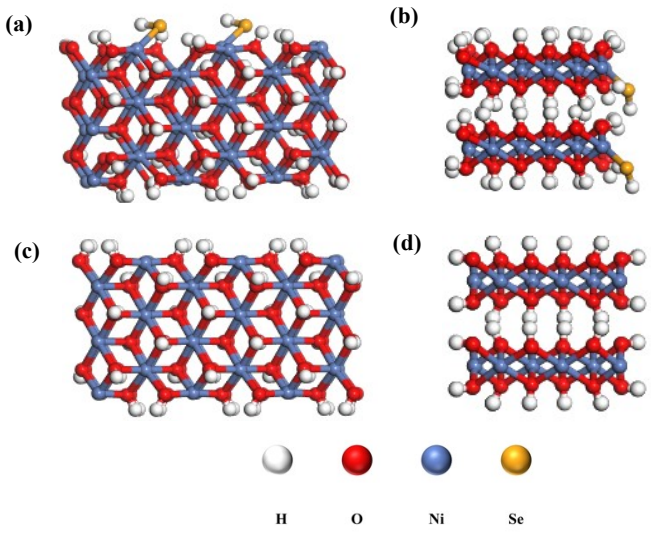

Fig. S11. The structural models of Se-$Ni(OH)_2$ (a,b),and $Ni(OH)_2$ (c, d).

Table S1. The binding energy of Ni 2p for $Ni(OH)_2$ and Se-$Ni(OH)_2$.

Catalysis	Binding energy/eV			
	Ni $2p_{3/2}$		Ni $2p_{1/2}$	
	Ni^{2+}	Satellite	Ni^{2+}	Satellite
$Ni(OH)_2$	855.46	861.20	873.02	879.09
Se-$Ni(OH)_2$	855.73	861.25	873.29	879.37

Table S2. Comparison of UOR performance of Se-$Ni(OH)_2$ with some other catalysts.

Electrode	Potential(V)	Scan rate (mV s^{-1})	Reference electrode	Urea concentration (mol dm^{-3})	Oxidation current density (mA cm^{-2})	Reference
Se-$Ni(OH)_2$	1.35	10	RHE	0.33	116.7	this work
$NiSe_2/MoSe_2$	1.54	10	RHE	0.33	100.7	[8]
β-$Ni(OH)_2$-CNTs	0.80	50	SCE	0.33	98.5	[9]
$NiMoO_4$-C	1.54	10	RHE	0.33	96.5	[10]
$NiO_{0.85}Se$/rGO	1.60	5	RHE	0.50	98.0	[11]
CoGC	0.60	20	Ag/AgCl	0.33	6.4	[12]
$NiMoO_4/C_{ps}$	0.60	10	Ag/AgCl	0.33	16.0	[13]
NiF_2/NiP_2	1.35	10	RHE	0.33	160	[14]
$Ni_{95}Pt_5$/C	0.65	20	Hg/HgO	0.33	30.9	[15]
Ni-NiO/Gr-450°C	0.50	10	SCE	0.33	38.2	[16]

RHE: relative hydrogen electrode

SCE: saturated calomel electrode

Table S3. The energies involved in urea and CO_2 molecule adsorption on the surface of Se-$Ni(OH)_2$ and $Ni(OH)_2$ catalysts.

Structure	$E_{A/surf}$/eV	E_{surf}/ eV	$E_{A(g)}$/eV	E_{ads}/eV
Se-$Ni(OH)_2$-urea	-82180.4	-80963.8	-1215.48	-1.12267
$Ni(OH)_2$-urea	-82531.1	-81315.3	-1215.48	-0.33967
Se-$Ni(OH)_2$-CO_2	-81991.8	-80963.8	-1027.91	-0.07050
$Ni(OH)_2$-CO_2	-82344.7	-81315.3	-1027.91	-1.55719

References

1. D. Yang, Y. Gu, X. Yu, Z. Lin, H. Xue and L. Feng, *ChemElectroChem*, 2018, **5**, 659-664.
2. L. Feng, X. Zhao, J. Yang, W. Xing and C. Liu, *Catal. Commun.*, 2011, **14**, 10-14.
3. X. Ruan, X. Cui, G. Jia, J. Wu, J. Zhao, D. J. Singh, Y. Liu, H. Zhang, L. Zhang and W. Zheng, *Chem. Eng. J.*, 2022, **428**,132579.
4. J. Li, S. Sun, Y. Yang, Y. Dai, B. Zhang and L. Feng, *Chem. Commun.*, 2022, **58**, 9552-9555.
5. H. Liu, P. Wang, X. Qi, A. Yin, Y. Wang, Y. Ye, J. Luo, Z. Ren, S. Yu and J. Wei, *Chem. Eng. J.*, 2024, **491**.
6. X. Yu, Z.-Y. Yu, X.-L. Zhang, P. Li, B. Sun, X. Gao, K. Yan, H. Liu, Y. Duan, M.-R. Gao, G. Wang and S.-H. Yu, *Nano Energy*, 2020, **71**.
7. S. Chakrabarty, I. Offen-Polak, T. Y. Burshtein, E. M. Farber, L. Kornblum and D. Eisenberg, *J. Solid Stat Electr.*, 2020, **25**, 159-171.
8. C. Yin, F. L. Yang, S. L. Wang and L. G. Feng, *Chinese J. Catal.*, 2023, **51**, 225-236.
9. K. Premnath, P. Arunachalam, M. S. Amer, J. Madhavan and A. M. Al-Mayouf, *Int. J. Hydrogen Energ*, 2019, **44**, 22796-22805.
10. D. W. Yang, L. T. Yang, L. Zhong, X. Yu and L. G. Feng, *Electrochim. Acta*, 2019, **295**, 524-531.
11. C. X. Zhao, J. N. Liu, B. Q. Li, D. Ren, X. Chen, J. Yu and Q. Zhang, *Adv. Funct.Mater.*, 2020, **30**, 202003619.
12. N. Alotaibi, H. H. Hammud, N. Al Otaibi and T. Prakasam, *ACS. Omega.*, 2020, **5**, 26038-26048.
13. R. Miki, T. Yamaki, M. Uchida and H. Natsume, *Colloid Surface A*, 2022, **648**, 129418.
14. H. Liu, Z. Liu and L. Feng, *Nanoscale*, 2019, **11**, 16017-16025.
15. J. R. Barbosa, C. H. Paranhos, O. C. Alves, N. R. Checca, J. P. Serna, A. L. Rossi and J. C. M. Silva, *Electrochim. Acta.*, 2020, **355**, 136752.
16. S. Wang, P. Xu, J. Tian, Z. Liu and L. Feng, *Electrochim. Acta.*, 2021, **370**, 137755.